Defence Research and Development Canada
Recherche et développement pour la défense Canada

Investigation into the utility of Pixon image reconstruction technique for the DRDC Coded Aperture X-ray Backscatter Imager

R. Puetter
Pixon LLC

Scientific Authority: A.A. Faust
Defence R&D Canada – Suffield

Contract Report
DRDC Suffield CR 2005-122
June 2005

Canada

Investigation into the utility of the Pixon image reconstruction technique for the DRDC Coded Aperture X-ray Backscatter Imager

Pixon LLC
PO Box 312
East Setauket NY USA
11733-0312

Contract Number: W7702-04-R036/001/EDM

Contract Scientific Authority: A.A. Faust (403-544-5362)

Defence R&D Canada – Suffield

Contract Report

DRDC Suffield CR 2005-122

June 2005

FINAL REPORT

Investigation into the Utility of the Pixon Image Reconstruction Technique for the DRDC Coded Aperture X-ray Backscatter Imager

Richard Puetter, Principal Investigator

Pixon LLC
P.O. Box 312
East Setauket NY 11733-0312
619-227-2739
Rick.Puetter@pixon.com

1. Executive Summary

- Monte Carlo calculations were performed to determine the theoretical limit on radiometric and positional accuracy for coded aperture measurement of point sources.
- For constant target illumination, set such that 10^6 counts would be collected on the focal plane when the focal plane was 6.86 cm from the target (i.e., the target is 3.43 cm in front of the mask), the accuracies are:
  - Radiometric: ~1.5% at 3.43 cm to ~3% at 34 cm
  - x- and y-accuracy: ~0.1 cm at 3.43 cm to ~3 cm at 34 cm
  - z-accuracy: better than ~0.1 cm from 3.43 cm to 34 cm. Does not seem to be a strong function of distance at least within this range of distances.

2. Introduction

In 2002 the UCSD High Energy Astronomy group formed a collaboration with Defence R&D Canada – Suffield (Dr. Anthony Faust) to use an energy-sensitive coded aperture X-ray detector developed at UCSD as the basis for a backscatter imaging system for one-sided imaging of IEDs and, eventually, AP mines. While the use of backscattered X-rays allows the photon source to be on the same side of the object as the detector, backscattering efficiency is usually poor. Further, the desire to have a portable system again reduces the intensity of available high-energy illumination sources. Consequently extremely photon-efficient imagers are required. Probably the most direct means of addressing these needs is by the use of a coded-aperture camera. However, because the multiple entrance apertures in such cameras produce many overlapping images, image reconstruction is required in order to see an image interpretable by the human eye. The current camera performs image reconstruction by convolution of the data with inverse masks, and takes advantage of developments in coded mask medical imaging—mask/antimask summation. Initial proof of concept tests with laboratory

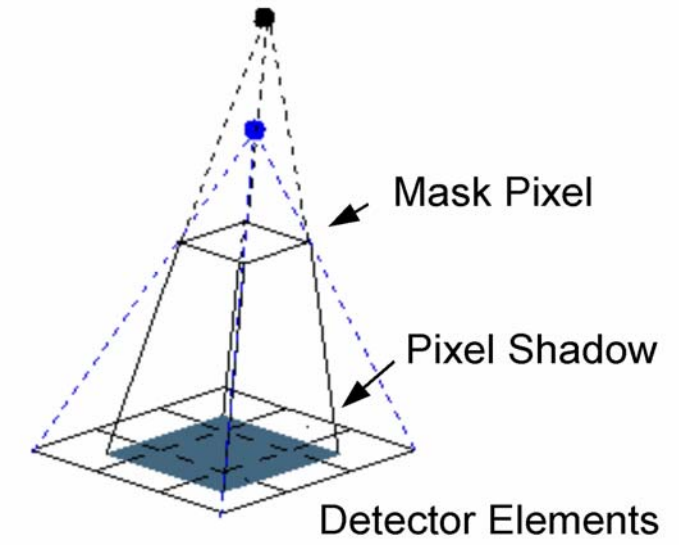

Figure 1. *Illustration of the capability of x-ray backscatter camera to provide 3-D information regarding the sample being probed. More distant sources (black dot) produce smaller images on the focal plane than do closer sources (blue dot). Such information can be used to determine the 3-D position of sources.*

detectors proved to be very encouraging.

In addition to obtaining planar images, x-ray backscatter camera also offer the ability to provide 3-D imaging. This capability is illustrated in Figure 1. As can be seen from the figure, identical sources placed at different locations form images on the focal plane of different sizes and positions. This information can be used to provide 3-D images of the sources illuminated by the backscatter camera. The primary goal of this project is to evaluate the utility of more sophisticated image processing techniques to obtain accurate 3-D information from coded aperture cameras. Specifically as a first step the current project focused on point source images with a goal of determining the theoretical limit of radiometric and 3-D positional accuracies obtainable with such a camera. The results of this study are presented in §5.

3. Coded Aperture Camera

A schematic diagram of the optical layout of the camera is shown in Figure 2. A diagram of the hole pattern in the mask is shown in Figure 3. The mask is a 2x2 array of a MURA mask with N=23. The pitch of the mask (linear dimension of the smallest square) is 0.0865 cm. The distance from the mask to the detector array (the focal length) is 3.43 cm. The detector is an array of CZT detectors (128x128 pixels) with a detector size of 0.05 cm.

4. Monte Carlo Calculation

To determine the positional and radiometric accuracy a geometric model of the camera was built in software. The model was for point sources with arbitrary brightness, and x-, y-, and z-positions. Rays from the point source were projected down onto the focal plane. The position of the projection of the mask holes was calculated and the flux from each hole divided between the appropriate pixels on the focal plane. The target was held at a constant illumination with a source brightness such that the focal plane would collect on average 10^6 counts in a standard exposure when the target was 6.86 cm from the focal plane, i.e., 3.43 cm in front of the mask. Exposure times were held constant and the geometric dilution of the flux ($1/r^2$) and dilution by geometric foreshortening ($\cos\theta$, where θ is the angle between the ray and the focal place) were accounted for as the camera was moved further and further away from the target. This gave rise to an exact mathematical description of the expected focal plane response for a point source at any arbitrary position.

To determine the radiometric and positional accuracy in the presence of random noise, in this case with a Poisson distribution, 40 noise realizations were calculated for each of 9 positions along the z-axis. For each data set a parametric point source model (brightness, x-, y-, and z-position) was fit to minimize the value of χ^2 using conjugate gradient minimization. The

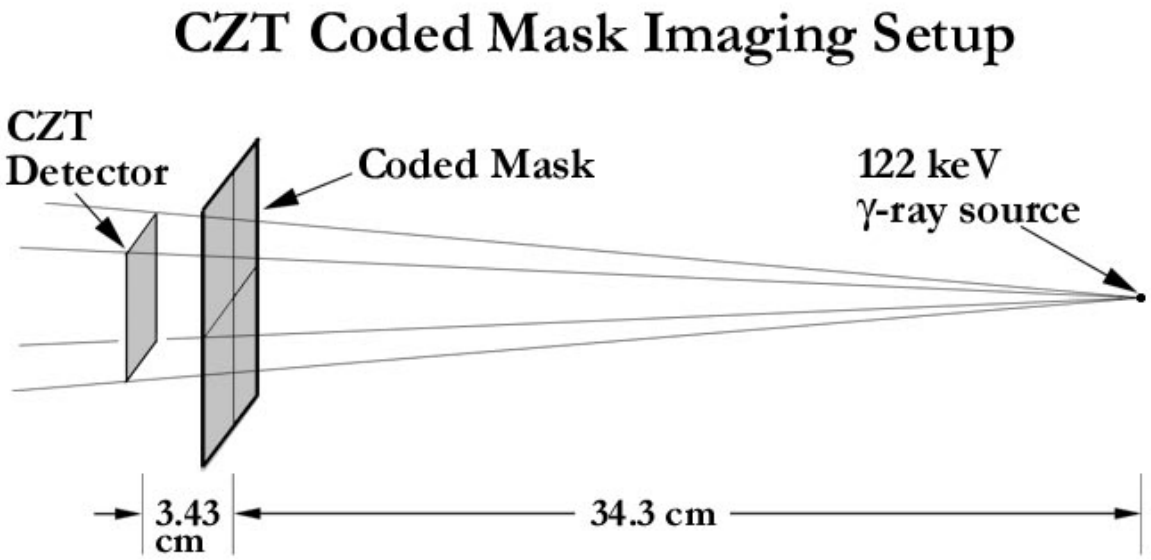

Figure 2. *Optical arrangement of the coded mask camera.*

average brightness and x-, y-, and z-positions and their standard deviation where then calculated from the model fits.

5. Results

Results of the Monte Carlo calculations appear in Table 1 and in Figures 4 through 11. In each figure the blue "+{ symbols present the 40 different results of the fits at each of the 9 z-positions selected along the z-axis. Specific details of the Monte Carlo results are given below.

Radiometry. The results of the Monte Carlo calculation for relative radiometric bias and relative accuracy are presented in Figures 4 and 5 respectively. (Absolute bias and accuracies are listed in Table 1.) As can be seen from Figure 4, the radiometric results seem unbiased and lie well within the accuracy values. An unexpected result is the relative insensitivity of the radiometric accuracy as a function of distance of the source from the mask. For the range of distances here, the flux collected on the focal plane varies by a factor of ~25. From pure counting statistics, the error at 3.43 cm from the mask should be 10^3 counts. The actual measured error is ~5 times this value. Such a large value can be understood because of the positional uncertainty of the source. For example, with a 0.05 cm

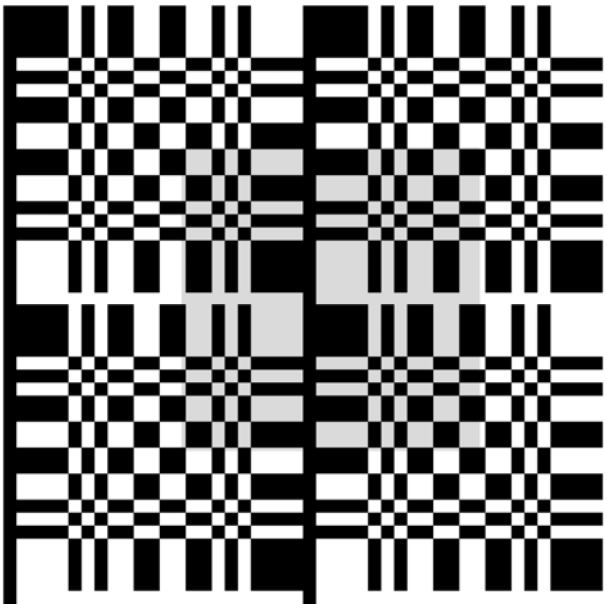

Figure 3. *2x2 array of an N=23 MURA array as is currently used in the UCSD X-ray Backscatter camera. The mask pitch (linear dimension of the smallest square) is 0.0865 cm.*

TABLE 1: Monte Carlo Results Summary									
Truth Values									
x-position	0.0	0.0	0.0	0.0	0.0	0.0	0.0	0.0	0.0
y-position	0.0	0.0	0.0	0.0	0.0	0.0	0.0	0.0	0.0
z-position	6.86	10.29	13.72	17.25	20.58	24.01	27.44	30.87	34.3
Counts[1]	1.0e6	1.0e6	1.0e6	1.0e6	1.0e6	1.0e6	1.0e6	1.0e6	1.0e6
Fit Values									
x-position	-0.0028	-0.0036	-0.0039	0.0406	0.0085	-0.1369	0.0402	0.0138	-0.1261
x-std. dev.	0.0102	0.0336	0.0899	0.2020	0.4422	0.6769	0.8037	1.134	2.729
y-position	-0.0016	-0.0117	0.0042	0.0559	0.0127	0.0922	-0.2596	-0.1425	-0.1605
y-std. dev.	0.0101	0.0339	0.0867	0.2282	0.4018	0.5007	1.106	1.519	2.472
z-position	6.852	10.24	13.68	17.15	20.59	24.01	27.44	30.87	34.32
z-std. dev.	0.0313	0.1017	0.0898	0.0220	0.0389	0.02777	0.0414	0.0432	0.1048
Counts	9.981e5	9.907e5	9.952e5	1.001e6	1.003e6	1.002e6	1.002e6	1.007e6	1.024e6
Cnt-std. dev.	7.295e3	1.793e4	1.185e4	3.668e3	6.457e3	6.405e3	6.862e3	10.14e4	2.848e4

[1]The value for the counts is referred to how many counts would be received by the focal plane if the target, which is receiving constant illumination, were placed at a distance of 6.86 cm from the focal plane (3.43 cm from the mask). The actual counts received at other distances are diluted by greater distance of the detector ($1/r^2$).

uncertainty in the z-position at 10,29 cm from the mask (second z-position calculated), the uncertainty in the source brightness from this alone would be about 9700 counts. This dominates the photon counting uncertain, which would be the only error if the source distance was known, and essentially reproduces the measured accuracy.

Another interesting feature is the fact that the radiometric accuracy is not a monotonic function of the distance of the source along the z-axis. Further, looking at the distribution of the individual fits (blue "+" symbols), this does not seem to be due to random errors, but a real feature presumably associated with the details of the mask and the way the illuminated holes are projected onto the focal plane pixels. Note that the various up and down motions of the black curve in Figure 5 are mimicked in Figure 11, which plots the positional accuracy in the z-position. This, of course, is not surprising since as we have just shown, the radiometric accuracy is strongly coupled to the z-positional accuracy. A potential subject for additional study would be to investigate the origin of this non-monotonic behavior.

X- and Y-Positional Bias and Accuracy. Figures 6 and 7 present the absolute positional bias and accuracies in the x-position and Figure 8 and 9 present the same quantities for the y-positions. The *absolute* biases and accuracies are presented for the x- and y-positions, since the truth values for these parameters are zero. Note while these curves are more monotonic than the radiometric bias accuracy, these curves also show significant structure. In addition, the x- and y-curves show significantly different dependencies. Again we assume this is due to details of the mask since the mask is not symmetric when rotated by 90°.

Relative Z-Positional Accuracy. Finally Figures 10 and 11 present the relative z-positional bias and accuracy. (Absolute bias and accuracy numbers are available in Table 1.) The coupling of the values presented here and the radiometric accuracies present in Figure 5 has already been discussed. However it seems peculiar to us that the z-positional accuracy seems relatively insensitive to distance, at least over the range explored here, but apparently

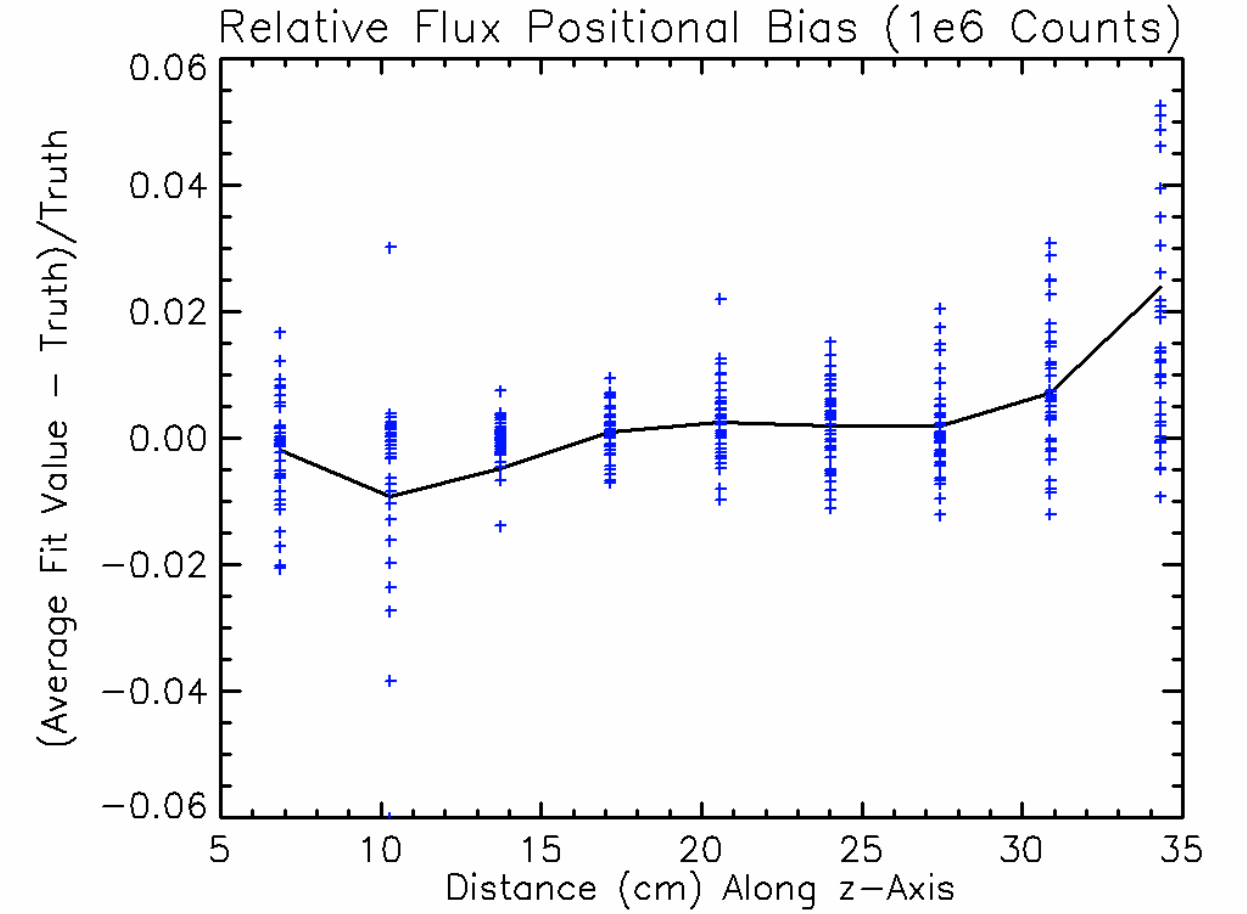

Figure 4. *Count bias. Plotted is the average value (black curve) of the fit to the counts for the 40 different noise realizations. The illumination on the target is held constant and set such that the focal plane would collect 106 counts when the target is 6.86 cm away (3.43 cm in front of the mask). The blue "+" symbols represent the fit value for the counts from each of the noise realizations.*

quite sensitive to details of how the illuminated holes project onto the focal plane. Nonetheless, the resulting positional accuracy is quite good. For all distances explored here the accuracy is better than ~0.1 cm.

6. Conclusions and Future Directions

Our study has demonstrated that MURA x-ray cameras can accurately measure the z-position of point sources. In fact the position can be determined very accurately. Surprisingly many of the details of the various positional and radiometric accuracies seems to depend on the particulars of the mask. Further work will be required to understand these dependencies. Before beginning such an investigation, however, we recommend that studies be done with real-life data. This is because we suspect that systematic errors will be more important in limiting resolution than the theoretical effects discussed here. Another important aspect will be exploring 3D reconstructions of extended objects. To perform reconstruction of such objects will probably require pre-calculation and storage of the PRFs since they change so strongly with z-position. The computational burden of such an approach should be compared to more common tomographic techniques.

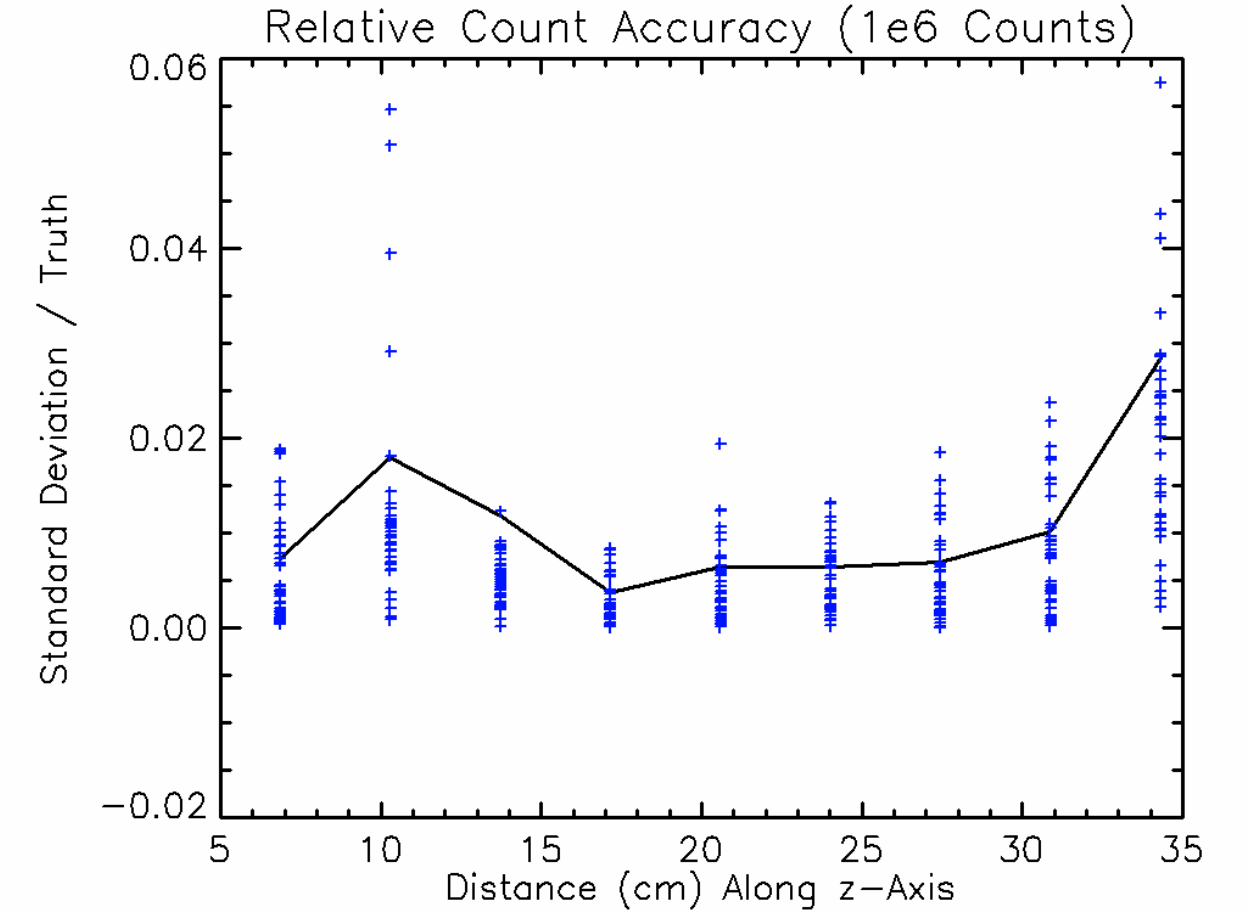

Figure 5. *Relative radiometric accuracy on the z-axis as a function of distance. The black curve shows the standard deviation divided by the true counts at each distance along the z-axis. The blue "+" symbols plot the absolute value of the deviation of each of the 40 fit points divided by the truth value so the reader can judge the range of fit values that were obtained.*

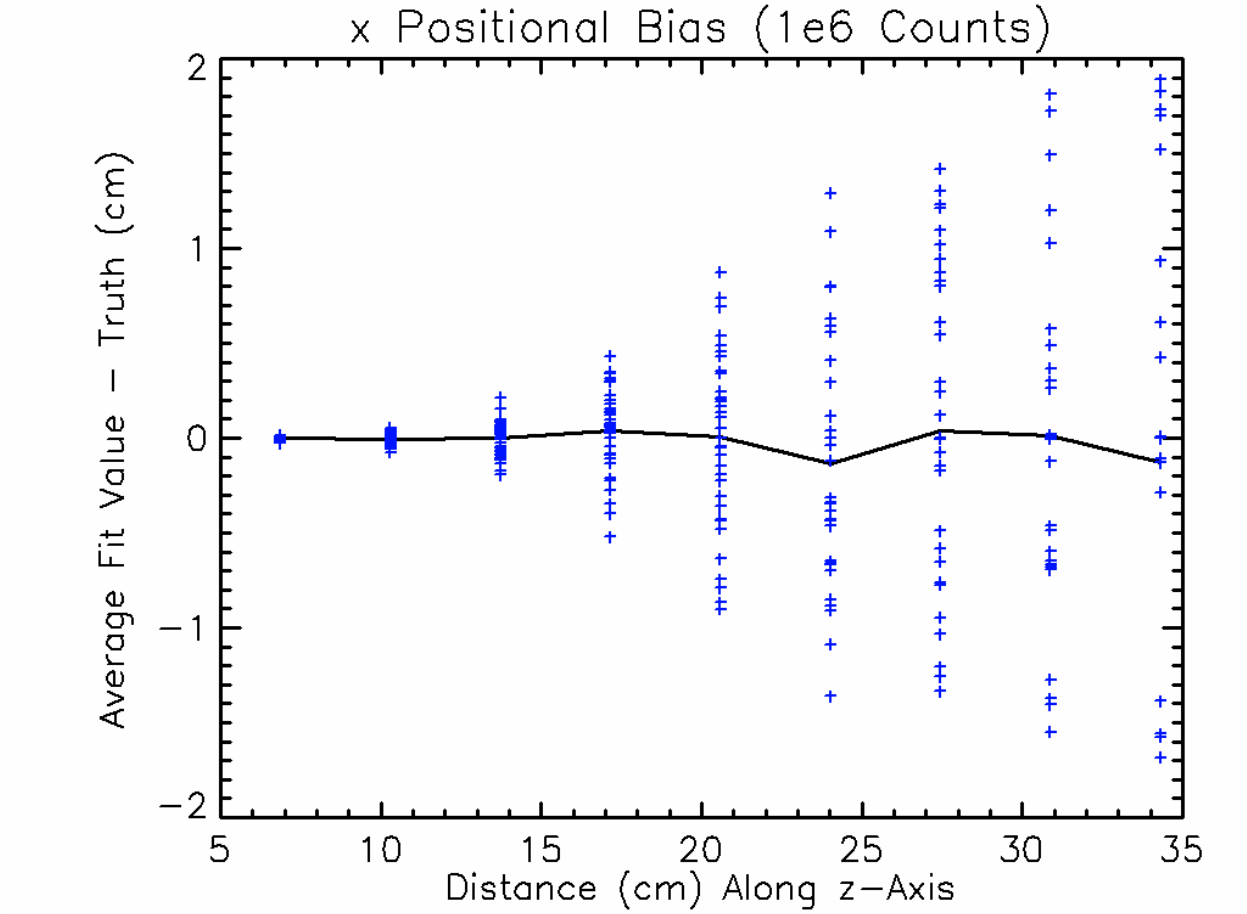

Figure 6. *x-position bias. Plotted is the average value (black curve) of the fit to the x-position for the 40 different noise realizations. The illumination on the target is held constant and set such that the focal plane would collect 106 counts when the target is 6.86 cm away (3.43 cm in front of the mask). The blue "+" symbols represent the fit value for the counts from each of the noise realizations.*

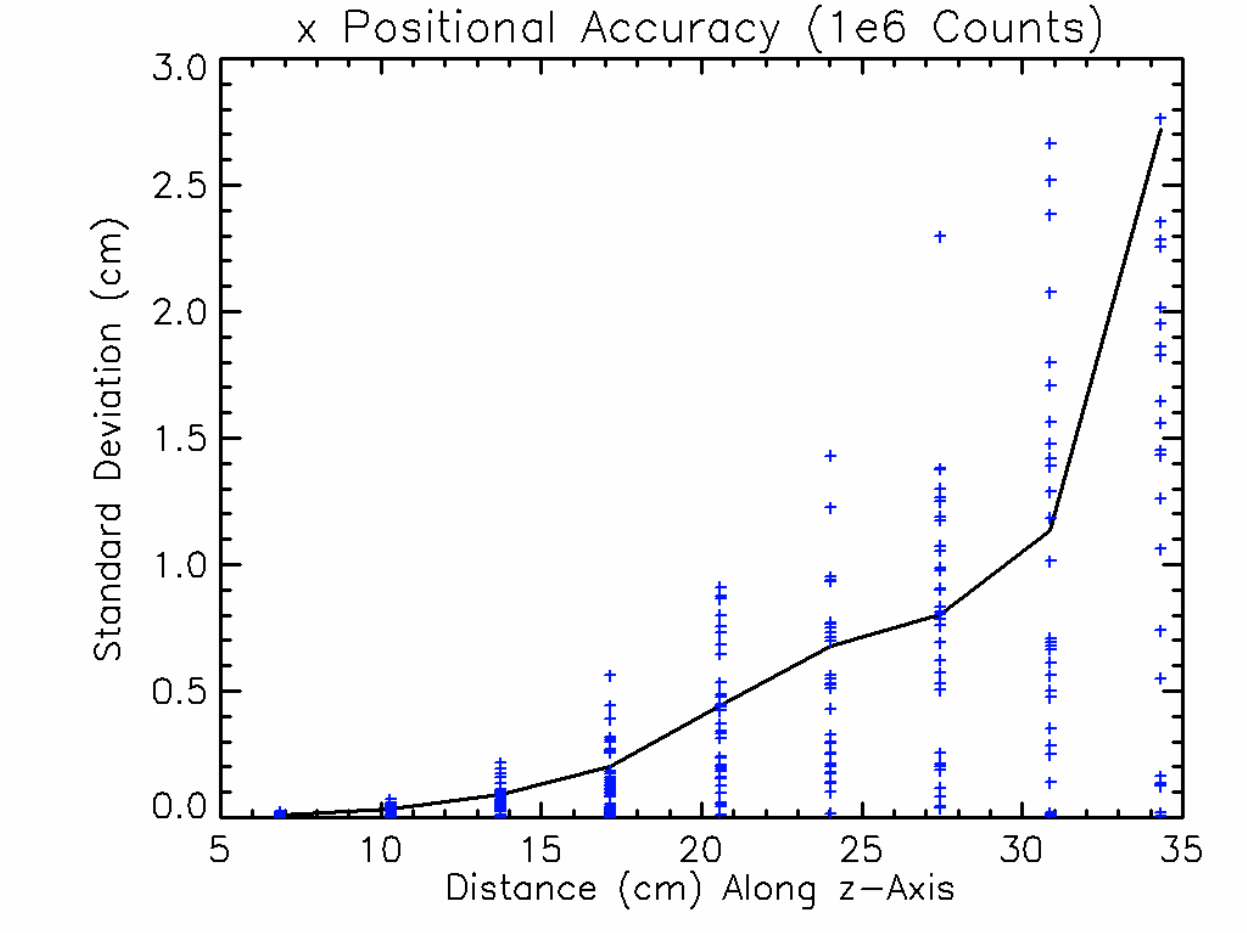

Figure 7. *x-positional accuracy on the z-axis as a function of distance. The black curve shows the standard deviation of the x-position at each distance along the z-axis. The blue "+" symbols plot the absolute value of the deviation of each of the 40 fit points so the reader can judge the range of fit values that were obtained.*

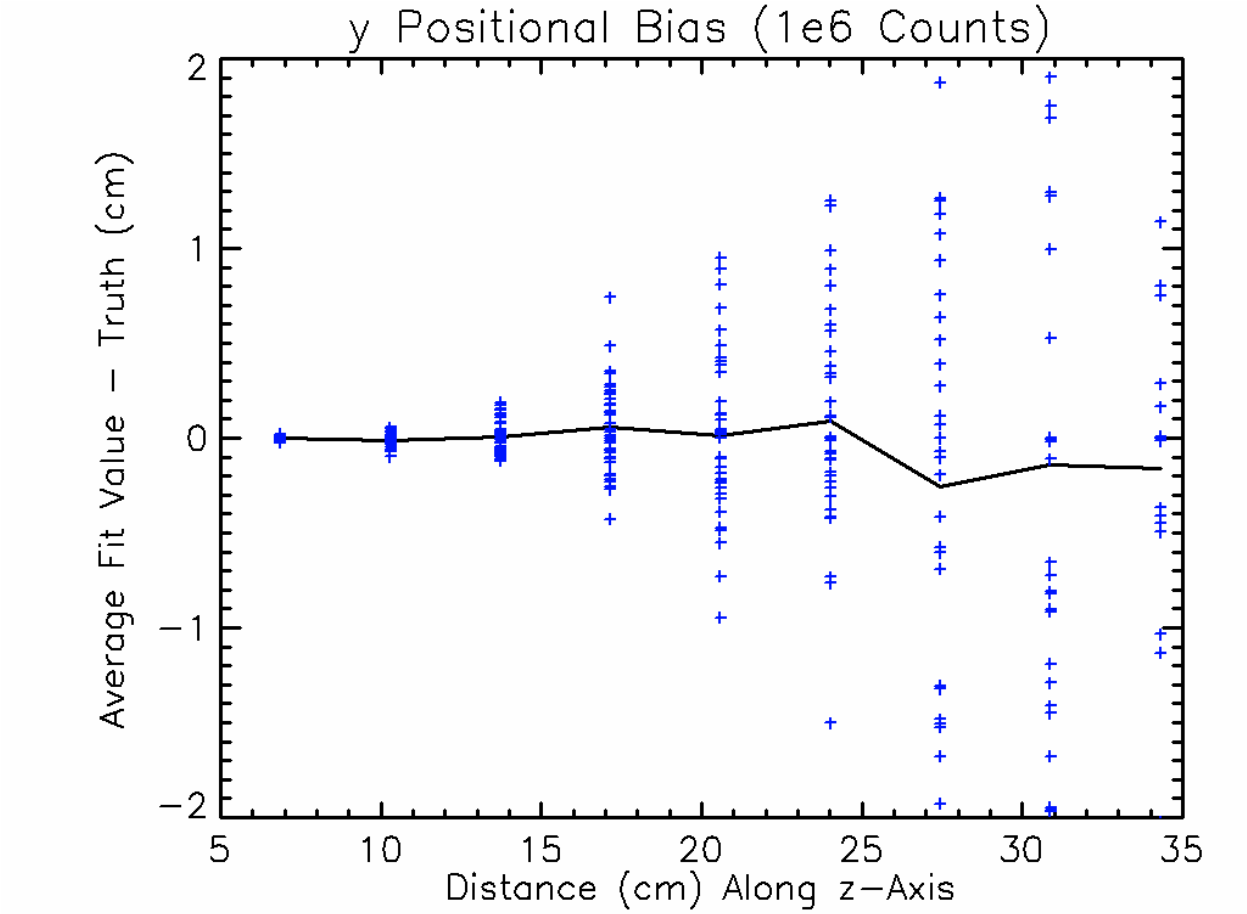

Figure 8. *y-position bias. Plotted is the average value (black curve) of the fit to the y-position for the 40 different noise realizations. The illumination on the target is held constant and set such that the focal plane would collect 106 counts when the target is 6.86 cm away (3.43 cm in front of the mask). The blue "+" symbols represent the fit value for the counts from each of the noise realizations.*

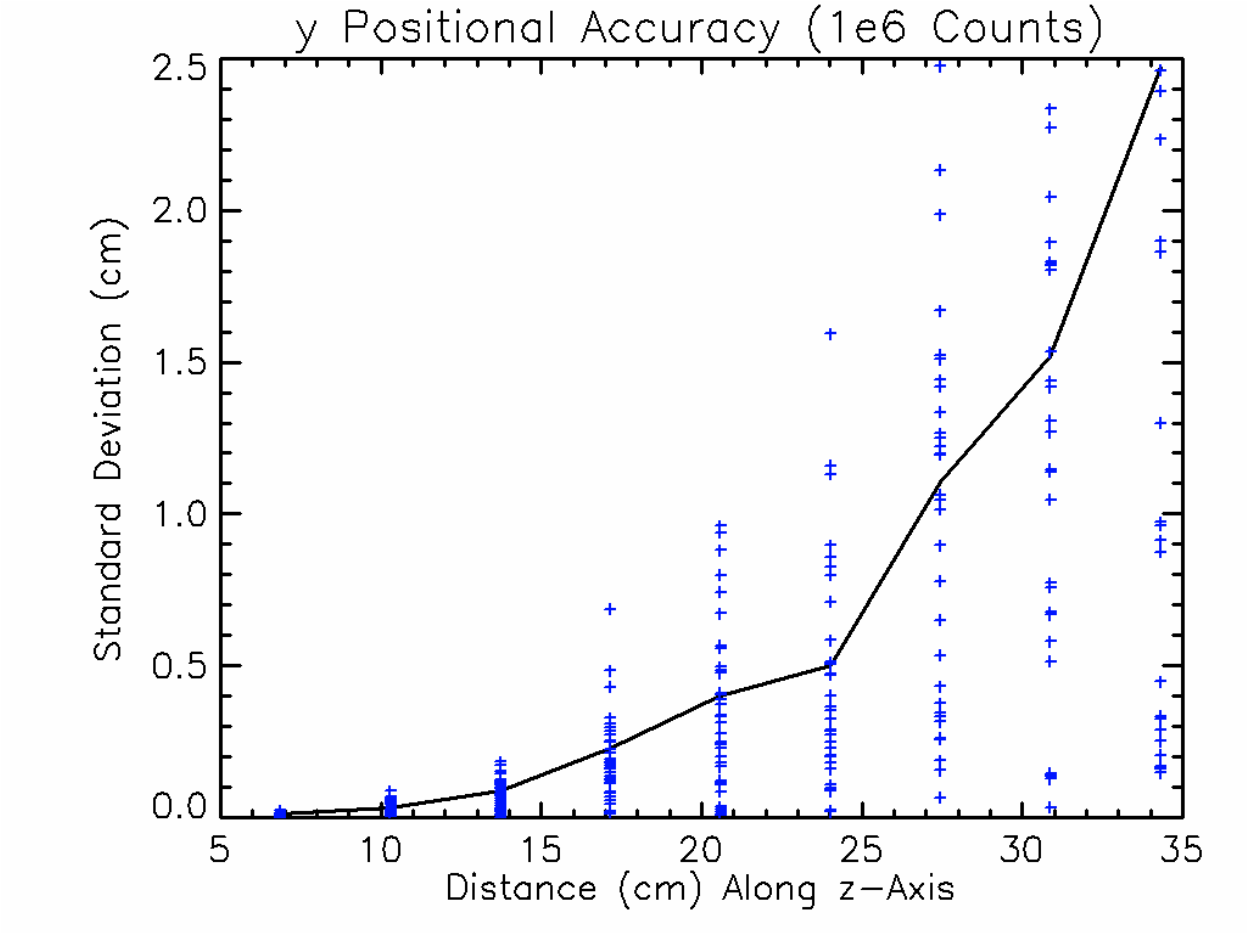

Figure 9. *y-positional accuracy on the z-axis as a function of distance. The black curve shows the standard deviation of the y-position at each distance along the z-axis. The blue "+" symbols plot the absolute value of the deviation of each of the 40 fit so the reader can judge the range of fit values that were obtained.*

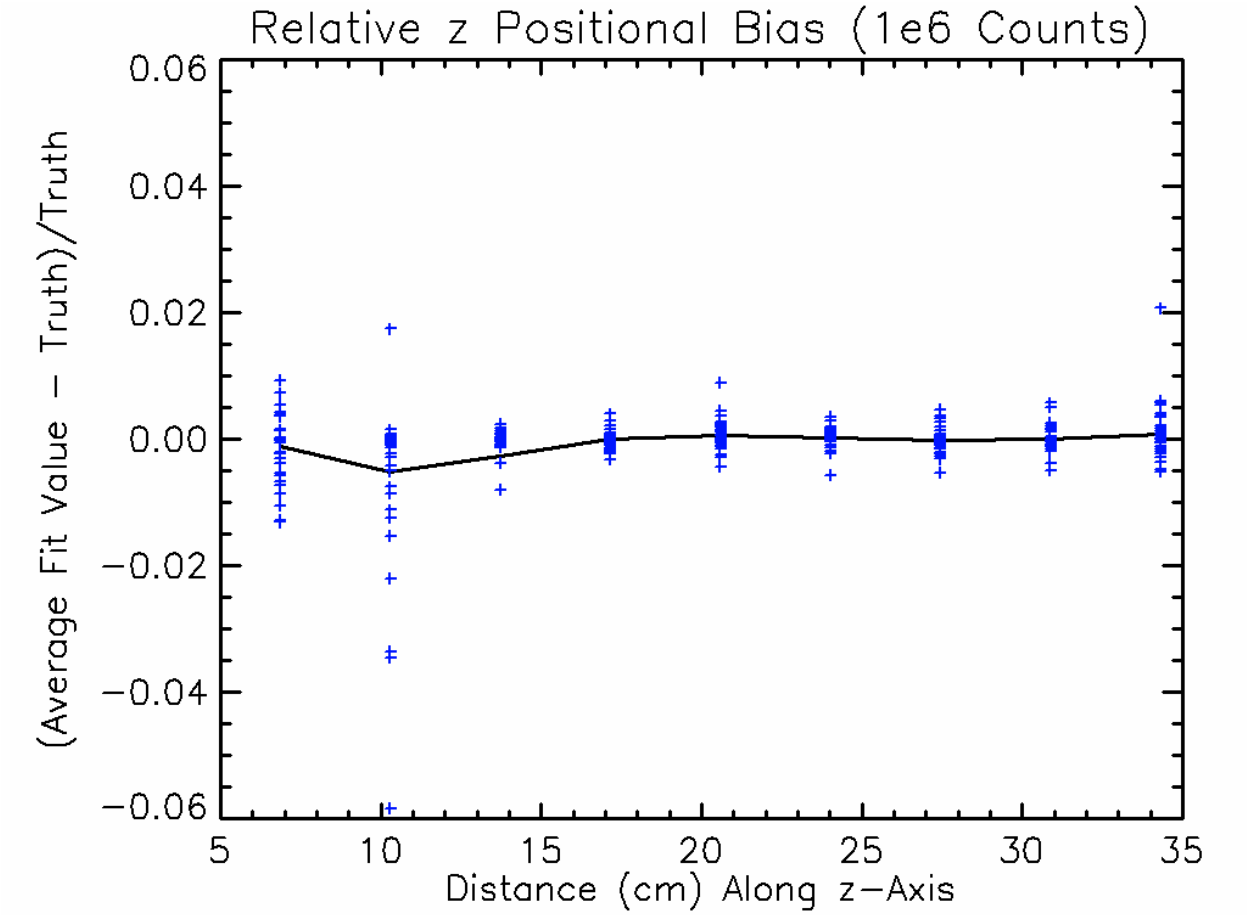

Figure 10. *z-position bias. Plotted is the average value (black curve) of the fit to the z-position for the 40 different noise realizations. The illumination on the target is held constant and set such that the focal plane would collect 106 counts when the target is 6.86 cm away (3.43 cm in front of the mask). The blue "+" symbols represent the fit value for the counts from each of the noise realizations.*

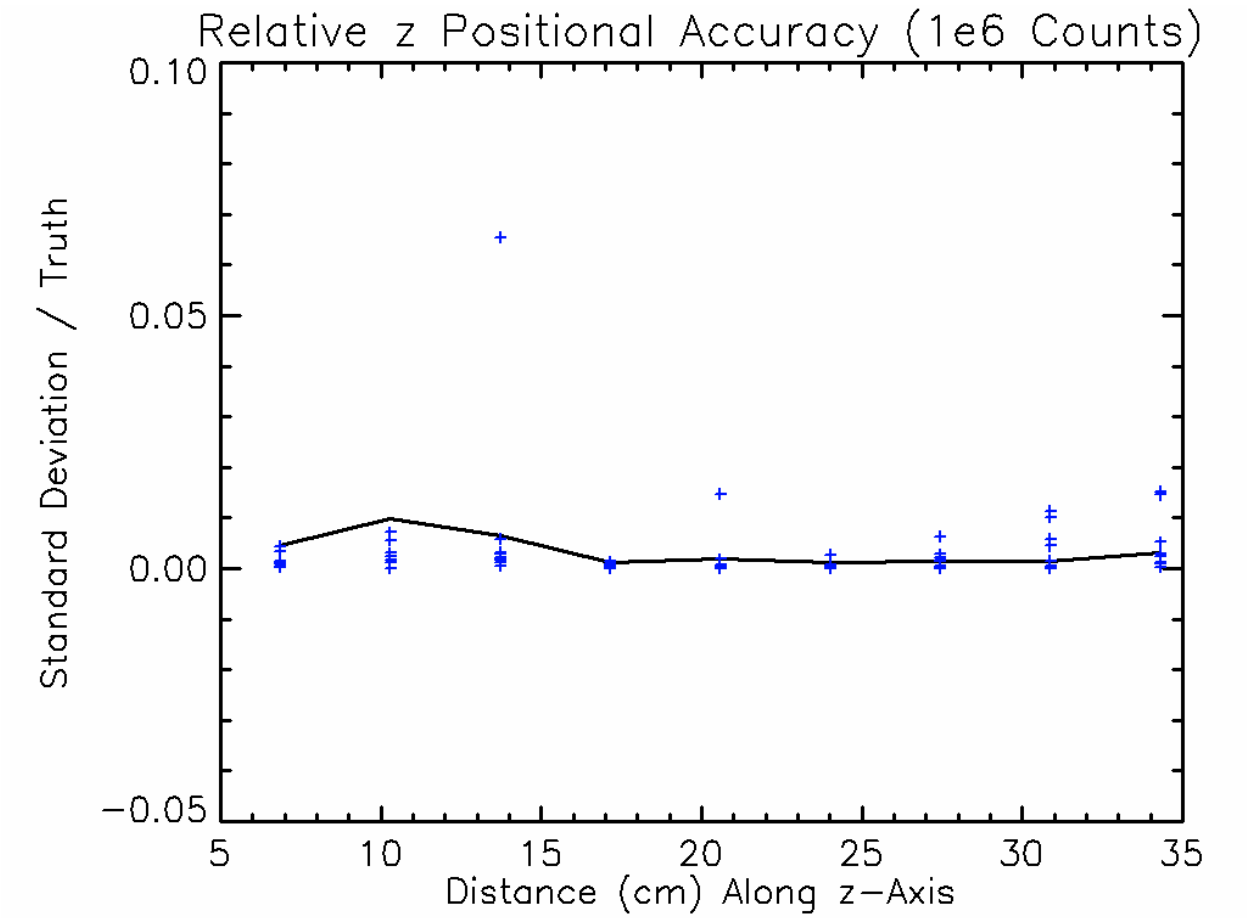

Figure 11. *Relative z-positional accuracy on the z-axis as a function of distance. The black curve shows the standard deviation of the z-position divided by the true value at each distance along the z-axis. The blue "+" symbols plot the absolute value of the deviation of each of the 40 fit points divided by the truth value so the reader can judge the range of fit values that were obtained.*

DOCUMENT CONTROL DATA

(Security classification of title, body of abstract and indexing annotation must be entered when the overall document is classified)

1. ORIGINATOR (the name and address of the organization preparing the document. Organizations for who the document was prepared, e.g. Establishment sponsoring a contractor's report, or tasking agency, are entered in Section 8.)

   Pixon LLC
   PO Box 312
   East Setauket NY USA 11733-0312

2. SECURITY CLASSIFICATION
   (overall security classification of the document, including special warning terms if applicable)

   Unclassified

3. TITLE (the complete document title as indicated on the title page. Its classification should be indicated by the appropriate abbreviation (S, C or U) in parentheses after the title).

   Investigation into the utility of the Pixon image reconstruction technique for the DRDC Coded Aperture X-ray Backscatter Imager (U)

4. AUTHORS (Last name, first name, middle initial. If military, show rank, e.g. Doe, Maj. John E.)

   Pixon LLC

5. DATE OF PUBLICATION (month and year of publication of document)

   June 2005

6a. NO. OF PAGES (total containing information, include Annexes, Appendices, etc) 20

6b. NO. OF REFS (total cited in document) 0

7. DESCRIPTIVE NOTES (the category of the document, e.g. technical report, technical note or memorandum. If appropriate, enter the type of report, e.g. interim, progress, summary, annual or final. Give the inclusive dates when a specific reporting period is covered.)

   Contract Report

8. SPONSORING ACTIVITY (the name of the department project office or laboratory sponsoring the research and development. Include the address.)

   Defence R&D Canada – Suffield, PO Box 4000 Station Main, Medicine Hat, Alberta, Canada T1A 8K6

9a. PROJECT OR GRANT NO. (If appropriate, the applicable research and development project or grant number under which the document was written. Please specify whether project or grant.)

9b. CONTRACT NO. (If appropriate, the applicable number under which the document was written.)

   W7702-04-R036/001/EDM

10a. ORIGINATOR'S DOCUMENT NUMBER (the official document number by which the document is identified by the originating activity. This number must be unique to this document.)

   DRDC Suffield CR 2005-122

10b. OTHER DOCUMENT NOs. (Any other numbers which may be assigned this document either by the originator or by the sponsor.)

11. DOCUMENT AVAILABILITY (any limitations on further dissemination of the document, other than those imposed by security classification)

   (x) Unlimited distribution
   ( ) Distribution limited to defence departments and defence contractors; further distribution only as approved
   ( ) Distribution limited to defence departments and Canadian defence contractors; further distribution only as approved
   ( ) Distribution limited to government departments and agencies; further distribution only as approved
   ( ) Distribution limited to defence departments; further distribution only as approved
   ( ) Other (please specify):

12. DOCUMENT ANNOUNCEMENT (any limitation to the bibliographic announcement of this document. This will normally corresponded to the Document Availability (11). However, where further distribution (beyond the audience specified in 11) is possible, a wider announcement audience may be selected).

   Unlimited

13. ABSTRACT (a brief and factual summary of the document. It may also appear elsewhere in the body of the document itself. It is highly desirable that the abstract of classified documents be unclassified. Each paragraph of the abstract shall begin with an indication of the security classification of the information in the paragraph (unless the document itself is unclassified) represented as (S), (C) or (U). It is not necessary to include here abstracts in both official languages unless the text is bilingual).

DRDC Suffield is developing a portable nuclear imaging technology that will provide sufficient speed, contrast and spatial resolution to enhance significantly the ability of Explosive Ordnance Detection (EOD) operators to identify and evaluate the internal construction of Improvised Explosive Devices (IED) and other suspicious objects. Based on the technique of Coded Aperture Imaging, this novel technology will only require access to a single side of a suspicious object, and will provide the ability to reconstruct images in depth. The latter feature is unique to this approach, and is quite unlike any other current field portable imaging techniques. While the depth reconstruction capability of the approach has been known for a few years, no one has yet demonstrated an algorithm that would efficiently reconstruct the 3D position of a target using the data available from a fixed mask-detector Coded Aperture design. One interesting approach to discern the depth information inherit in the Coded Aperture data maybe the Pixon method, which represents a new and innovative way of modelling an image in terms of its information content. This report details a feasibility study to ascertain the potential for the Pixon image analysis method to reconstruct the 3D position of targets using the data available from a Coded Aperture X-ray Backscatter Imager.

14. KEYWORDS, DESCRIPTORS or IDENTIFIERS (technically meaningful terms or short phrases that characterize a document and could be helpful in cataloguing the document. They should be selected so that no security classification is required. Identifies, such as equipment model designation, trade name, military project code name, geographic location may also be included. If possible keywords should be selected from a published thesaurus, e.g. Thesaurus of Engineering and Scientific Terms (TEST) and that thesaurus-identified. If it is not possible to select indexing terms which are Unclassified, the classification of each should be indicated as with the title.)

X-ray, Imaging, Coded Aperture, Landmine, IED, Explosive, Detection